Atomistic Simulations of Early Stage Clusters In Al-Mg Alloys

David Kleiven[a], Olve L. Ødegård[a], Kari Laasonen[b], Jaakko Akola[a,c]

[a]*Department of Physics, Norwegian University of Science and Technology (NTNU), NO-7491 Trondheim, Norway*
[b]*School of Chemical Technology, Aalto University, P.O. Box 16100, FI-00076, Aalto, Finland*
[c]*Laboratory of Physics, Tampere University of Technology, FI-33101 Tampere, Finland*

Abstract

The Cluster Expansion formalism based on Density Functional Theory (DFT) simulation data has been applied for Al-Mg alloys with high accuracy ($\sim$ 1 meV/atom). The atomistic simulations are used to model the Al-Mg phase diagram, phase boundaries and the initial solute clustering at different compositions and temperatures. The obtained free energies of formation for the FCC, HCP and γ-phase are in accordance with the experimental phase diagram. The calculations demonstrate the formation of Guinier-Preston (GP) zones of Al_3Mg ($L1_2$ phase) within the Al matrix under varying conditions. The computed transition temperatures where the ordered structures dissolve are approximately 50 K higher than experimental data. The free energy barriers associated with the formation of GP-zones increase as the solute (Mg) concentrations are reduced and the temperature is increased.

Keywords: Nucleation, Cluster Expansion, Microstructure, Atomistic Modelling, Aluminium alloys

1. Introduction

Aluminium and magnesium alloys play an important role in a variety of commercial products, including the aerospace and the automotive industries [1, 2]. The special set of Al-based alloys, denoted as the 6xxx (Al-Mg-Si) and 7xxx (Al-Mg-Zn) series, have been extensively studied experimentally due to their beneficial mechanical properties, such as high hardness and strength [3, 4, 5, 6, 7, 8]. The binary Al-Mg system forms the basis for all of these alloys providing thereby an important reference system, but the thermodynamics of the initial clustering of this system is not fully explored and there is a need for first-principle atomistic models.

The Cluster Expansion (CE) formalism [9] is an attractive method for studying thermodynamic properties of alloys, as it provides a parametrised energy model trained by data from Density Functional Theory (DFT) calculations (high accuracy). Energies of arbitrary configurations can thus be evaluated with a low computational effort, enabling statistical simulations of systems much larger than what is accessible via DFT while preserving the accuracy. CE has previously been used to study the thermodynamics of a range of systems, including Ni-Rh [10], Fe-Ni [11], Cu-Pd [12], Al-Sc [13], Mg-Nd [14] and many more [15].

In this work, we investigate three phases in the equilibrium phase diagram of Al-Mg, namely FCC, γ-phase and HCP. The intermetallic β-phase (around 30-40% of Mg) [16, 17] has important technological applications, but it has a complex structure with a unit cell of 1168 atoms. Furthermore, the β-phase shows several partially occupied and split positions which increase the complexity from a computational point of view. Due to these complications, the β-phase is considered out of scope for the present study. Here, we compute the temperature dependence of the solubility of Mg in Al and enthalpies of formation as a function of concentration and temperature. At last, we study the free energy barrier associated with the formation of Guinier-Preston (GP) zones in Al-rich solutions. GP zones are coherent clusters of solute atoms, formed in the early stages of the precipitation process, and thereby instrumental intermediates for precipitate formation [4, 18]. We show that a combination of CE with statistical Monte Carlo simulations provides an efficient method of extracting the free energy associated with the formation of GP zones. Understanding the initial clustering on the lattices of the bulk matrix is important for modelling precipitates, which further are critical in determining the mechanical properties of the alloy in question.

2. Theory

The Cluster Expansion (CE) expresses the total energy of a structure as [9]

$$E_{\mathrm{CE}} = \sum_{c_f} V_{c_f} \prod_{i \in c_f} \sigma_i, \tag{1}$$

where c_f denotes a cluster and i is the index of a site. In the case of the binary Al-Mg system, σ is a spin variable, where $\sigma_i = +1$ indicates that Al occupies site i, while $\sigma_i = -1$ indicates the same for Mg. V_{c_f} is the effective cluster interaction (ECI), which is fitted to total energy calculations. ECIs are obtained from a set of DFT calculations via the compressive sensing technique [19], where the objective function

$$S = \sum_{n=1}^{N} (E_{\mathrm{DFT,n}} - E_{\mathrm{CE,n}})^2 + \lambda \sum_{c_f} |V_{c_f}| \tag{2}$$

Email address: jaakko.akola@ntnu.no (Jaakko Akola)

is minimised. λ is a hyper parameter which is selected such that the leave-one-out cross-validation (LOOCV) [20] is minimised, N is the number of structures calculated with DFT, E_{DFT} is the energy from the DFT calculations and E_{CE} is the energy predicted by the CE in equation (1). The latter sum in equation (2) runs over all possible clusters. Here, all clusters up to four atoms within a cut-off radius of 4.96 Å are included. The LOOCV score is determined as follows: First, one of the structures is left out of the dataset. Then the ECIs are fitted to the total energies of the remaining structures. The deviation between the predicted energy from the DFT energy of the structure left out is collected. This procedure is repeated for all the structures in the dataset, and LOOCV is the average of all the deviations.

The thermodynamic properties of the Al-Mg systems are computed using Markov Chain Monte Carlo (MCMC) in the Semi Grand Canonical Ensemble (SGCE) [21] where the simulations are performed at fixed chemical potential μ, and in the canonical ensemble where the composition is fixed. In SGCE, the number of atoms is fixed but the composition may vary. The chemical potential is subtracted from ECI corresponding to the single atom cluster interactions

$$E_1 = V_1 \frac{1}{N} \sum_i \sigma_i \rightarrow (V_1 - \mu) \frac{1}{N} \sum_i \sigma_i. \tag{3}$$

The free energy F in the canonical ensemble is defined by

$$\exp(-\beta F) = Z, \tag{4}$$

where $\beta = 1/k_B T$, k_B is the Boltzmann constant, T is the temperature and Z is the partition function. From equation (4), the free energy can be computed from the exact differential

$$d(\beta F) = U d\beta, \tag{5}$$

where U is the internal energy. Exploiting that $\lim_{T\rightarrow\infty} \beta F = -\sum_i c_i \ln c_i$, where c_i is the concentration of species i, the free energy at an arbitrary temperature is given by

$$\beta F = -\sum_i c_i \ln c_i + \int_0^\beta d\beta' U(\beta'). \tag{6}$$

From the Monte Carlo results, the enthalpy of formation and the free energy of formation can be computed. The enthalpy of formation is defined as the enthalpy of a structure minus the weighted average of the enthalpies of the pure elements, and similarly for the free energy. In addition to identification of the stable phases, the concentration at which solute atoms form clusters, is a parameter of high interest. The solubility of Mg in Al can be computed by tracking the phase boundary between Al and Al_3Mg. In this context, solubility means the maximum concentration of Mg atoms that can be dispersed in the Al matrix before regions of ordered Al_3Mg ($L1_2$ phase) appear. Based on the requirement that the free energies at the same chemical potential in two co-existing phases have to be the same, one can derive the following equation for the evolution of chemical potential μ at the phase boundary with respect to inverse temperature β [22]

$$\frac{d\mu}{d\beta} = \frac{U_\xi - U_\alpha}{\beta(x_\xi - x_\alpha)} - \frac{\mu}{\beta}. \tag{7}$$

$U_{\xi(\alpha)}$ is the internal energy and $x_{\xi(\alpha)} = \langle \sum_i \sigma_i / N \rangle_{\xi(\alpha)}$ is the thermal averaged singlet correlation function in each phase ξ and α. N is the total number of atoms in the simulation cell. Starting from two phases at low temperature, equation (7) can be integrated towards high temperatures. The initial condition at zero temperature is $\mu(T = 0) = (U_\xi - U_\alpha)/(x_\xi - x_\alpha)$, which can be obtained by requiring that $d\mu/d\beta = 0$ at zero temperature.

We solve equation (7) by applying an adaptive forward Euler scheme: Two MC simulations are kept in memory, one in phase ξ and one in phase α. The thermal averaged energy $U_{\xi(\alpha)}$ and singlet terms $x_{\xi(\alpha)}$ can therefore be computed on each step. At low temperature, the compositions in the two phases do not change much, so the first steps can easily be computed. As the temperature rises, a method for deciding if the inverse temperature step size should be refined or not is needed. We achieve this by fitting a smoothed cubic spline to the singlet curves $x_\xi(T)$ and $x_\alpha(T)$ obtained so far. The splines are used to extrapolate the relevant singlets for the next temperature. After each step, the obtained singlet values are compared to the values predicted by the splines. If the computed values deviate by more than a predefined threshold (we use here 0.05) the system is reset to a previous state and the inverse temperature step size is reduced by a factor two. Once a step is accepted, the splines are updated to take into account the already known new singlet values. As the two phases are sampled at the co-existence line, one of the systems might spuriously change phase. Therefore, we also reduce the step size if the compositions of the two phases become similar. When the step size $\Delta\beta$ reaches a pre-set minimum value, the calculation terminates; we used a minimum step size corresponding to 1 K. The two systems are equilibrated on each step.

Besides calculating the phase boundaries, we also study formation energetics of ordered Guinier-Preston zones within the aluminium matrix. If the growth of the GP zone is sufficiently slow, one can study the growth in a quasi-static approximation where the atoms are assumed to occupy sites according to the Boltzmann distribution at any time during the growth process. According to the classical nucleation theory [23], the free energy associated with a particular size is given by

$$\Delta G = -\Delta g N + \kappa N_{\mathrm{surf}}, \tag{8}$$

where Δg is the difference in free energy of the pure phases, N is the number of solute atoms in the GP zone, κ is an energy cost associated with the interface between the GP zone and the matrix and N_{surf} is the number of atoms on the interface. As pointed out by Kamijo *et al.*, there is also an energy cost associated with the change in entropy, which can be considerably larger than the interface contribution if the zone is highly coherent with the surrounding matrix [24]. The theoretical framework developed by Kamijo *et al.* has previously been used to compute the free energy barrier of Cu precipitation in an iron matrix [25]. Correspondingly, the present computational approach consists of evaluating the enthalpy difference between N Mg atoms fully dissolved in the Al-matrix and the cluster with the lowest energy formed by the same atoms. The entropy

difference is approximated by

$$\Delta S = k_B(N-1)\ln c_{\mathrm{Mg}}, \tag{9}$$

where c_{Mg} is the initial solute concentration [24].

In addition to the energy cost associated with changing entropy, there can be significant contributions from strain fields. The strain fields originates from the lattice mismatch between the matrix material and precipitating phase. By assuming that the precipitate is ellipsoidal, such energy contributions can be estimated from Eshelby's inclusion theory [26]. We obtain the elastic tensors of the matrix material and the precipitating phase via DFT calculations by perturbing the simulation cell around the minimum energy shape and calculate the resulting stress tensor [27].

We now proceed to address some technical issues with the γ-phase where we observed a very low acceptance rate in the MC simulations while sampling configurations. This indicates that the energy changes from the vast majority of trial moves are considerably larger than the thermal energy in the system (corresponding to a deep energy funnel). To extract the weak temperature dependence of enthalpies and free energies in the case of very low acceptance rates, we apply a mean field approach. First, we find the ground state by simulated annealing, and then we compute the partition function of the system directly by restricting the possible configurations to the ones that can be formed by swapping *only* two atoms from the ground state. If the system consists of n_{Al} aluminium atoms and n_{Mg} magnesium atoms, each aluminium atom can be swapped with all magnesium atoms resulting in $n_{\mathrm{Al}} \times n_{\mathrm{Mg}}$ configurations to be considered.

3. Simulation Details

The total energies used to train the cluster expansion model were obtained from DFT calculations using the GPAW program [28, 29, 30] in the plane-wave (PW) mode with 500 eV as the kinetic energy cut-off and the Perdew-Burke-Ernzerhof (PBE) functional for the exchange-correlation energy [31]. The Brillouin zone was sampled using a $4 \times 4 \times 4$ Monkhorst-Pack grid in a unit cell of 64 atoms. All structures and cells were fully relaxed until the forces were below 0.05 eV Å^{-1} and stresses below 0.003 eV Å^{-3}. For Al-Mg alloys, the energy change during relaxation is substantial due to the large difference in lattice parameters. For example, the FCC lattice parameter for 35 atomic percent Mg is 4% larger than that of pure aluminium [32]. We apply the cluster expansion module implemented in ASE [33] to obtain the ECIs. To select structures for DFT calculations, we combine the ground state search with the variance minimising technique proposed by Seko *et al.* [20]. We point out that no structure was rejected due to severe relaxation artefacts or other criteria, and thus the obtained CE model is based on all the structures generated by the previously mentioned strategies. In order to obtain sufficient accuracy for stress tensor, we use a kinetic energy cutoff of 800 eV.

The system was equilibrated in all Monte Carlo simulations as follows: The average energy was obtained from M samples resulting in a value E_1. Next, the sampled data were erased and the energy was again sampled for the same number of steps resulting in a value E_2. If E_1 and E_2 are equal within the statistical fluctuations, the system is considered to be in thermodynamic equilibrium. The sampling continues until the mean values in two successive "windows" of size M are equal within the uncertainty. Here, a window size corresponding to ten times the number of atoms was used. The correlation time τ was determined using the approach of Van de Walle *et al.* [22], and the variance $\bar{\sigma}^2$ used for comparing E_1 and E_2 was given by

$$\bar{\sigma}^2 = \frac{2\tau\sigma^2}{N}, \tag{10}$$

where σ^2 is the observed variance and N is the number of samples.

Thermal averaged quantities were obtained by adding samples until the standard deviation of the mean value reached a predefined threshold with a specified statistical significance, i.e.

$$\bar{\sigma} < \frac{p}{z_\alpha}, \tag{11}$$

where p is the threshold z_α is the percentage of a normal distribution for a confidence level α.

During MC simulations the size of regions of "connected" atoms can be tracked. For instance, connected atoms can stand for a group of solute atoms linked by nearest-neighbour bonds. We construct such networks using the tree structure proposed by Newman and Ziff [34]. Throughout this work, we use Mg-Mg pairs connected with second nearest-neighbour bonds as indicators for clustering.

4. Results

ECIs obtained for Al-Mg in FCC are shown in figure 1. The corresponding leave-one-out cross-validation is very small, only 1.05 meV/atom. ECIs comprise important detailed information of the energetics within an alloy. Here, ECI for the nearest-neighbour interaction is positive and the second nearest-neighbour interaction is negative. Combining this with the signs of the spin variables σ where Al and Mg are +1 and -1, respectively, leads to a conclusion that the elements have a tendency to mix based on energetics.

MC simulations were carried out in a $10 \times 10 \times 10$ expansion of the primitive FCC cell to compute the enthalpy of formation at different temperatures, and the results are shown in figure 1b. There is a qualitative change in the curve shapes after 430 K, where the three local minima of the ordered structures are still visible, while there are no signs of local minima at 505 K. The ordered structures Al_3Mg (corresponding to the $L1_2$ phase), AlMg ($L1_0$) and $AlMg_3$ ($L1_2$ reversed), shown in figure 1c, are pronounced as anticipated from the pair interactions in figure 1a.

The $\mu - T$ phase boundary separating Al and Al_3Mg, obtained from equation (7), is shown in figure 2a. Compositions in the two phases were computed at each point on the $\mu - T$ line. A conversion of the $\mu - T$ phase diagram in figure 2a to a

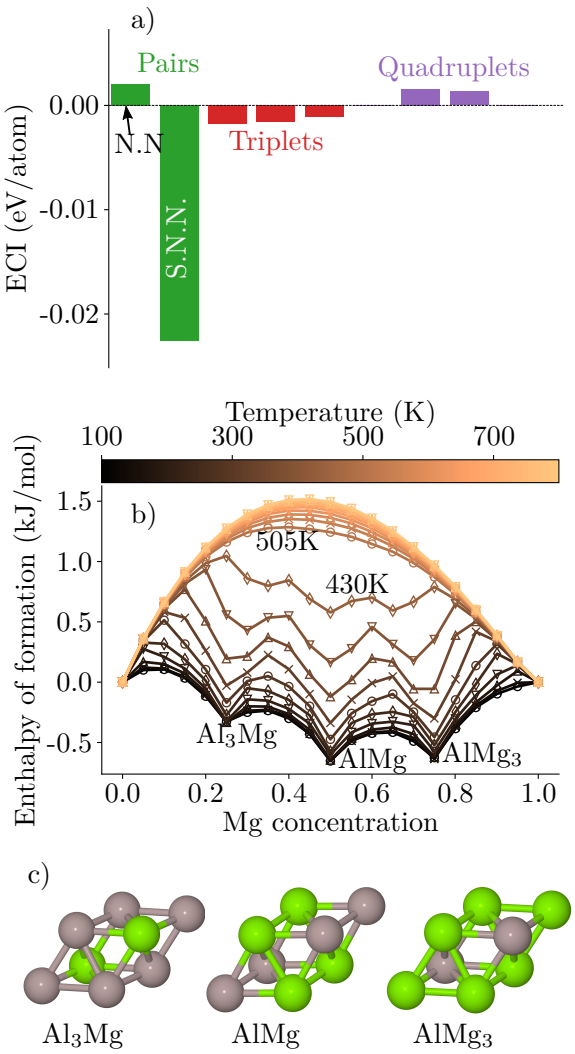

Figure 1: *a)* ECIs obtained for Al-Mg in FCC, excluding the singlet and the bias terms. N.N. refers to nearest-neighbour interactions and S.N.N. refers to second nearest-neighbour interactions. *b)* Enthalpy of formation at different temperatures on the FCC lattice, indicated by the colour scale. The reference energies are pure Al and Mg on FCC. *c)* Low energy structures Al_3Mg, AlMg and $AlMg_3$. Colour code: Grey, aluminium; green, Mg.

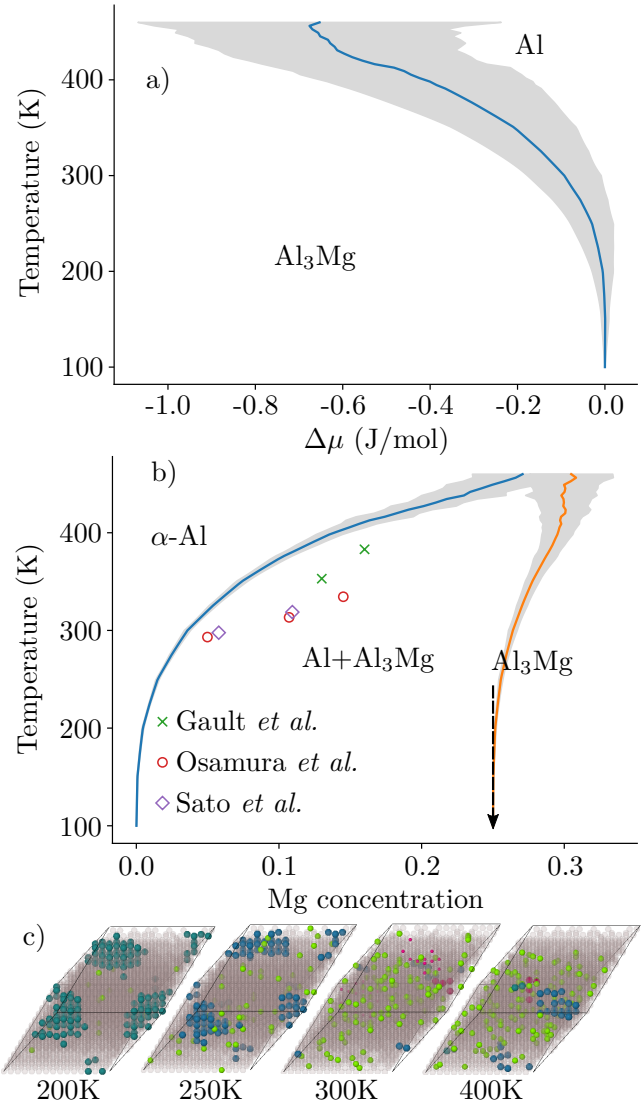

Figure 2: Phase boundary obtained by solving equation (7). *a)* The solid line is the mean of 100 runs and the shaded region indicates one standard deviation. The x-axis gives the change in chemical potential from its value at 100 K. *b)* Composition temperature phase diagram obtained by converting the $\mu-T$ phase boundary in figure *a*. The points are experimental measurements [35, 36, 37]. The blue and orange curves are the average composition on the $\mu-T$ curve when starting from pure Al and Al_3Mg, respectively. *c)* Snapshots from MC simulations of 3375 times expanded primitive unit cell. The systems are shown at different temperatures and the overall Mg concentration is 5%. The highlighted atoms are Mg atoms belonging to the same cluster (identified by colour), except the light green ones which represents Mg atoms *not* belonging to a cluster of size 4 or larger.

composition-temperature phase diagram, is shown in figure 2b. Here, the blue curve corresponds to the thermal averaged composition on the $\mu - T$ line in figure 2a when starting from pure Al and the orange line represents the same starting from Al_3Mg. Gault *et al.* studied the temperature at which GP zones become unstable using ultrasonic measurements, and they found that GP zones become unstable at 13% Mg content at 80 °C and at 16% Mg content at 110 °C [35]. Osamura *et al.* extracted the dissolution temperature of GP zones from differential scanning calorimetric measurements [36], and Sato *et al.* found the maximum temperature at which GP zones are formed from resistivity measurements [37]. The experimental data points are included for comparison and they reveal that the calculations slightly overestimate the maximum temperatures.

The tendency of forming Al_3Mg clusters is apparent in the snapshots of the MC simulations in figure 2c. Highlighted atoms with the same colour represent Mg atoms in the same cluster, except light green which represents separated Mg atoms or atoms belong to a cluster smaller than four atoms. A cluster is defined as a region where the Mg atoms are second nearest-neighbours. At low temperatures nearly all Mg atoms belong to an extended region of Al_3Mg (with periodic boundary conditions), while several smaller zones form as the temperature increases, and eventually Mg becomes randomly dispersed in

the Al matrix.

4.1. γ-phase

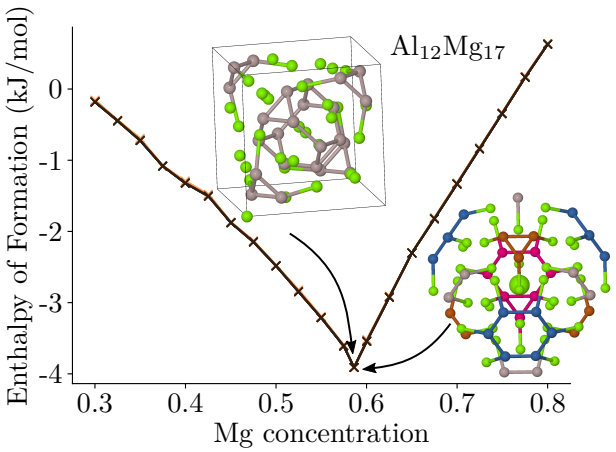

Figure 3: Computed enthalpy of formation using the mean field approximation described in the theory section. Colour code for upper inset: Mg, light green; Al, grey. Lower inset: Al is coloured by the distance from the central Mg atom. The order is pink, brown, blue and grey from closest to farthest.

At concentrations around 60% Mg, the lowest energy structure has the stoichiometric formula $Al_{12}Mg_{17}$, as shown in figure 3. The γ-phase belongs to space group 217 and has four symmetrically distinct sites. Here, we trained a cluster expansion model using the cell shown as the uppermost inset in figure 3, and achieved LOOCV of 6.7 meV/atom. The enthalpy of formation has been simulated for temperatures ranging from 200 K to 800 K, but we observe almost no effect of temperature in this range, indicating that the energy cost associated with swapping one Al-atom with one of the Mg-atoms is much larger than the thermal energies considered. The uppermost inset in figure 3, shows the ground state in the 58 atom cell used for DFT calculations, while the lower right inset shows how Al is distributed around the central Mg atom.

4.2. Mg-rich Structures

The effective cluster interactions in the HCP lattice are shown in figure 4a. CE was trained with structures ranging from 25% to 100% Mg content, due to difficulties in getting the cross-validation score down when including all structures down to pure Al in HCP (high-energy configurations). The LOOCV score for this set is 3.2 meV/atom. ECI corresponding to second nearest-neighbour is negative, suggesting that an ordered phase where second nearest-neighbours consists of similar elements is expected here as well.

The enthalpy of formation on the Mg-rich side, shown in figure 4b, was computed with MC simulations in a HCP cell containing 1000 atoms. The lowest enthalpy of formation is found at 75% Mg concentration. In contrast to FCC, there are no local minima at 50% and 25% of Mg. In this case, the temperature effect on curve shapes becomes visible after 468 K

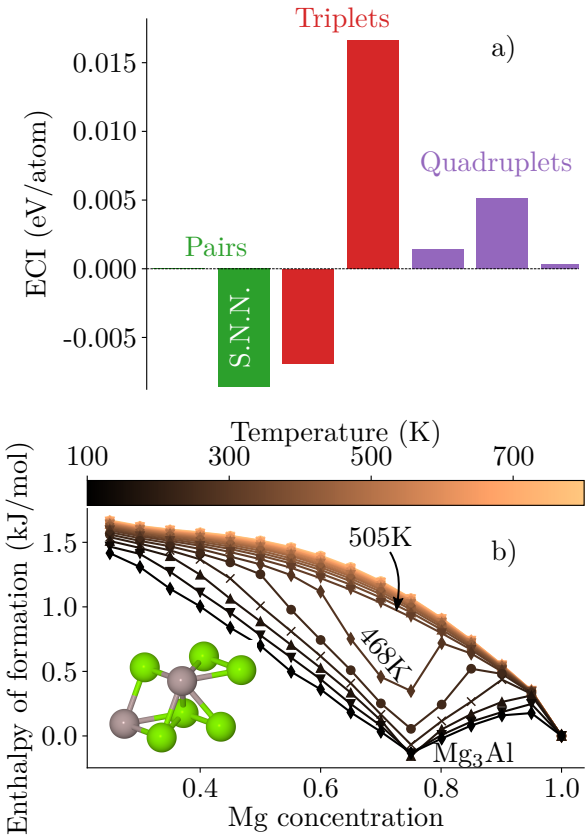

Figure 4: *a)* ECIs obtained for the HCP lattice. S.N.N. refers to second nearest neighbours. *b)* Enthalpy of formation as a function of temperature and composition. The reference energies were pure Al and Mg on HCP. The inset shows the Mg_3Al structure that has the lowest enthalpy of formation.

where there is one local minimum at 75% Mg concentration, whereas at 505 K the local minimum has disappeared.

The collected free energies of formation for the three phases and the formation energies of all DFT calculations in this study, are shown in figure 5. The reference energies correspond to pure Al and pure Mg, both in the FCC configuration, and the concentration dependent density changes are included for all phases. As expected, the free energy of formation is lower for HCP at high Mg concentrations ($>$ 80%) at all temperatures. However, the HCP free energy increases rapidly as the Mg concentration is lowered. For concentrations ranging from 35% to 75% Mg, the γ-phase has the lowest free energy. Note that we ignored HCP structures with less than 25% Mg content and included only γ-structures with Mg content in the range 30% – 80%. The ignored structures do not play any role when describing the thermodynamics of Al-Mg alloys due to their high free energy of formation. According to the experimental phase diagram, the Al-Mg system is known to be in a β-phase around 40% of Mg [16, 17]. This structure has more than 1000 atoms in the unit cell, and was considered as out of scope for this study due to the high computational cost associated with DFT calculations necessary for training the cluster expansion algorithm. Therefore, one should not expect a transition be-

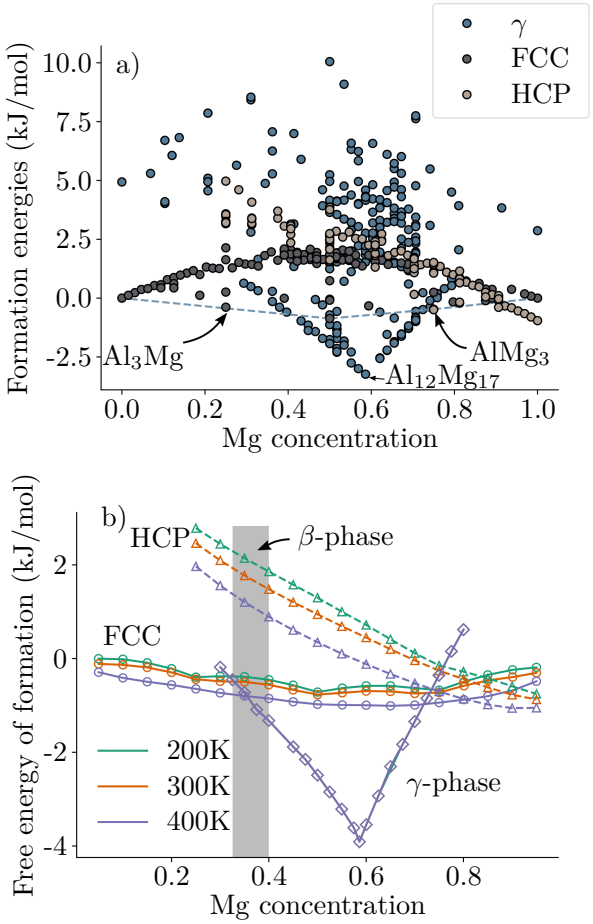

Figure 5: Comparison of energies in all the phases. *a)* All DFT energies obtained for the three phases. The dotted line denotes the convex hull for the FCC phase. *b)* Free energy of formation the HCP (triangles), FCC (circles) and γ-phase (diamonds) lattice.The temperature is indicated by the colour of the curve.

tween FCC and the γ-phase within the shaded region as the β-phase is not considered.

4.3. Nucleation of Al_3Mg zones

The elastic properties obtained for aluminium and the Al_3Mg phase in table 1, shows that the precipitating phase is much softer than the surrounding matrix. Moreover, we find that

Table 1: Elastic constants obtained in the present study and values obtained in two previous studies. B denotes the bulk modulus, G the shear modulus and ν is the Poisson's ratio in the two phases.

	Present	Fu *et al* [38]	Bakare *et al.* [39]
B_{Al_3Mg} (GPa)	59.5	64.0	66.4
G_{Al_3Mg} (GPa)	43.1	31.8	41.0
ν_{Al_3Mg} (-)	0.21	-	0.24
B_{Al} (GPa)	77.3	-	78.2
G_{Al} (GPa)	26.0	-	20.5
ν_{Al} (-)	0.35	-	0.38

the initial misfit strains is dilatational and corresponds to a hydrostatic compression of 2.3% of the Al_3Mg phase. By solving Eshelby's equations to obtain the equivalent eigenstrains [26], we find that the strain energy per precipitate volume is $w = 0.33\,\text{meV Å}^{-3}$, when a spherical inclusion is presumed.

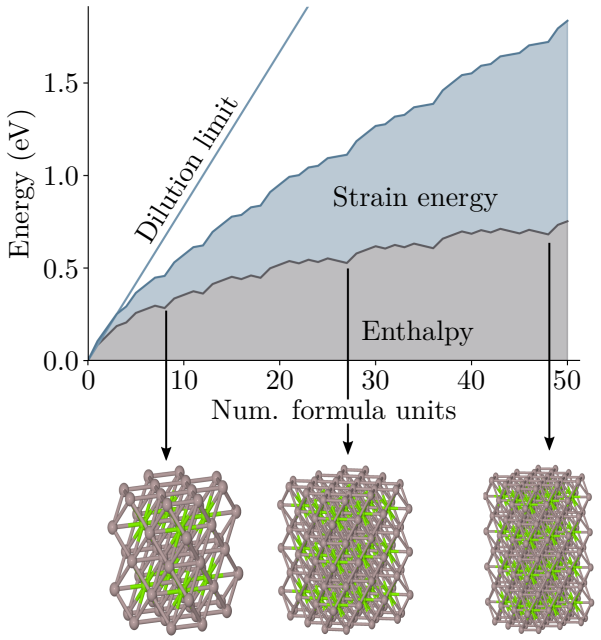

Figure 6: Energy of N Mg atoms forming a GP zone of Al_3Mg ($L1_2$). The blue straight line is the energy of N Mg atoms being dissolved in aluminium, and the grey and blue shaded regions represent energy and strain fields, respectively, of the cluster embedded in the Al-matrix. The insets are visualisations of special cluster sizes of 8, 27 and 36 atoms.

The enthalpy difference and the strain energy associated with the formation of a cluster of N Mg atoms is shown in figure 6. From Eshelby's inclusion theory, the strain contribution increase linearly with the volume of the inclusion. For all cluster

sizes, the energy of Al_3Mg clusters ($L1_2$ phase) is smaller than the energy of dissolved atoms, indicating that the interfacial energy between the Al_3Mg precipitate and the matrix is not large enough to produce an energy barrier. Moreover, it can be seen from the "bumps" on the energy curve that certain sizes give a particularly low energy. The low energy can be understood based on geometrical arguments which lead to particularly stable ("magic") cluster sizes: 8 Mg atoms form a cluster where they order in a cubic $2 \times 2 \times 2$ structure, while 12 atoms comprise a $2 \times 2 \times 3$ structure. Similarly for the sizes 27, 36 and 48, the stacking of Mg is $3 \times 3 \times 3$, $3 \times 3 \times 4$ and $3 \times 4 \times 4$, respectively. Three of these structures are illustrated in figure 6. We further note that the estimated strain energy is a significant contribution to the overall energy, but it does not destabilise the clusters.

Before calculating the free energy associated with cluster formation for a given size, we first show some pre-requisite results. At finite temperature, the Al_3Mg phase can be slightly distorted. Furthermore, when a cluster is embedded in a matrix, atoms on the cluster surface experience a local environment with fewer Mg second nearest neighbours than in the precipitate bulk. Consequently, we expect entropic contributions from surface distortions to play an active role starting at lower temperatures than disorder within the bulk.

The free energy and entropy associated with disordering of a perfect bulk Al_3Mg structure, was obtained by simulating a $10\times10\times10$ cell (25% Mg). Energetics related to the roughening of cluster surface is obtained from simulations where a Al_3Mg cluster is inserted into a bulk matrix of aluminium. During all MC steps in the latter calculation, Mg atoms were restricted to be connected to all other Mg atoms via second nearest neighbour bonds. Strain energy from the lattice mismatch between the phases, was not included in the MC runs. At 293 K, figure 7a shows that the entropy is clearly different from the value at 0K, indicating that the structure is not perfectly ordered. However, the entropy is far from its high temperature value, meaning that the cluster is still in the Al_3Mg phase. Figure 7b shows that already at low temperatures ($\sim$ 100 K) the clusters starts to deviate from the cubic ground state shape. Furthermore, at room temperature the smallest clusters reaches a plateau, indicating that all cluster shapes are visited, while the larger clusters remain far from their maximum entropy state. Snapshots from the MC calculations suggest that clusters with more rounded surfaces appear, provided that they are large enough not to reach their maximum entropy state at room temperature. Interestingly, we note that experiments show that Al_3Mg precipitates are spherical and not cubic, as the ground state. Deviations from the ground state can be understood based on the fact that the free energy is lowered when the surface has higher entropy [35]. A temperature induced rounding of Al_3Mg precipitates was also found in a previous study [40].

The free energy associated with the formation of a cluster (fig 8), consists of several terms. (a) The energy gain due to the lowering of the internal energy when the atoms order (fig 6), (b) an energy cost associated with interfacial interactions (c) strain fields and (d) the energy cost attributed to the lower entropy of the ordered structure. Due to the cost terms, the free

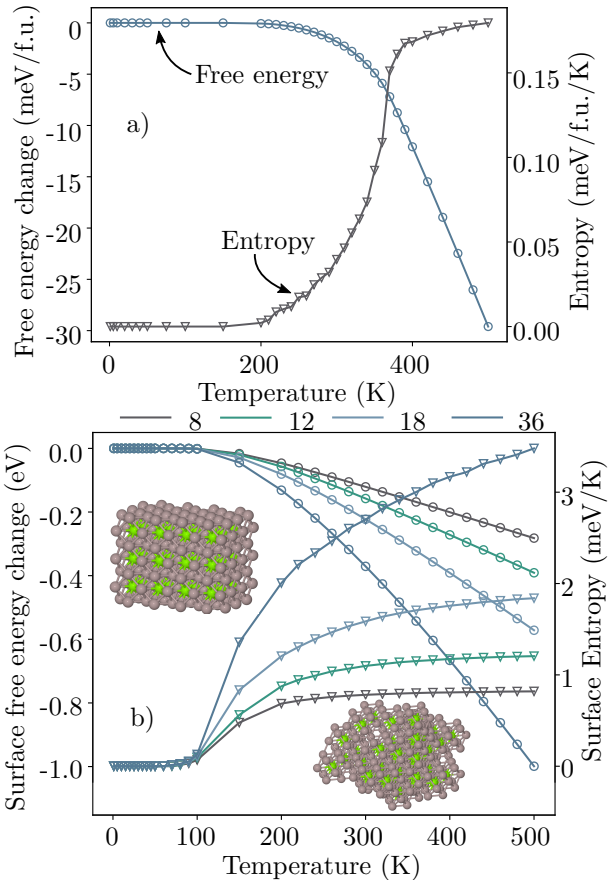

Figure 7: Free energy and entropy associated with *a)* deviations from a perfect Al_3Mg structure and *b)* deviations from the perfect cubical ground state cluster, while the defining property of Mg-Mg second nearest neighbour interactions is preserved. The inset in panel *b)* represent a 36 atom cluster at low temperature and at a snapshot at 300 K. Open circles denote free energy and open triangles entropy in both panels. The lower panel shows results for cluster sizes 8, 12, 18 and 36.

energy, as shown in figure 8a, increases until a critical cluster size is reached after which it decreases while adding more Mg atoms (nucleation). Hence, the system has to overcome a free energy barrier in order to form a large cluster, and this can be computed from the highest points of the curves shown in figure 8a. At 293 K, the entropic contribution from the cluster surface leads to a reduction of the barrier. In contrast, at 120 K we see that such contributions are negligible and the barrier is produced by the entropy change in Eq. (9). Furthermore, at 120 K a barrier can be seen at all compositions where the critical cluster size is 21, 5 and 3 formula units at 1%, 5% and 10%, respectively. We note that at 293 K for low Mg content, the critical size exceeds fifty Mg formula units, which is the largest size the chosen simulation box can host without severe artefacts from periodic boundary conditions. Consequently, the free energy barrier is much larger than the thermal energy at room temperature for such low solute concentrations. Our results show (figure 8b), that the free energy barrier for forming a GP zone increases with decreasing solute concentrations. Moreover, the barrier increases rapidly when the temperature rises.

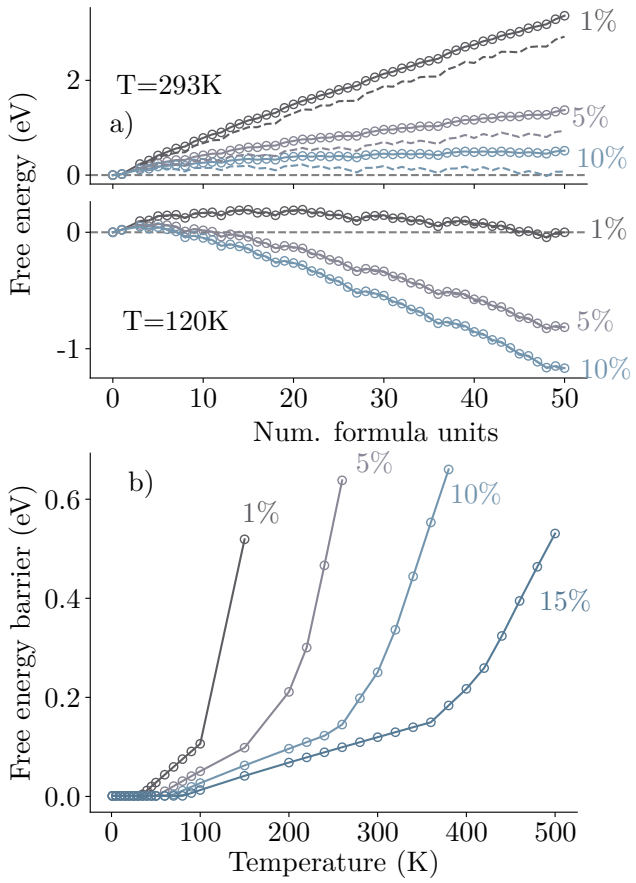

Figure 8: *a)* Free energy obtained with Kamijo's model (circular markers) and free energy including entropic contributions from the surface (dotted line) (Eq. (9) at 293 K and 120 K of systems where all Mg atoms are clustered together. The different colours corresponds to different initial solute concentrations. In both cases we include the strain energy from Eshelby's inclusion theory. *b)* Free energy barrier of GP zone formation. The colours represents different solute concentrations.

5. Discussion

The three ordered FCC structures Al_3Mg ($L1_2$ phase), AlMg ($L1_0$) and $AlMg_3$ ($L1_2$) have a lower enthalpy of formation compared to nearby concentrations in figure 1b. The precipitates being formed can be determined by considering three reactions

$$\begin{aligned} 3\,\mathrm{Al} + \mathrm{Mg} &\longrightarrow \mathrm{Al_3Mg}, \quad \Delta H_f = -0.33\,\mathrm{kJ\,mol^{-1}}, \\ \mathrm{Al} + \mathrm{Mg} &\longrightarrow \mathrm{AlMg}, \quad \Delta H_f = -0.65\,\mathrm{kJ\,mol^{-1}}, \\ \mathrm{Al} + 3\,\mathrm{Mg} &\longrightarrow \mathrm{AlMg_3}, \quad \Delta H_f = -0.64\,\mathrm{kJ\,mol^{-1}}, \end{aligned}$$

where the formation enthalpies are given at 100 K. In Al-rich alloys the number of magnesium atoms will be the limiting factor of the reaction. The first reaction "uses" the smallest amount of magnesium atoms meaning that more of this end product can be formed compared to the other two. Hence, the number of moles of atoms associated with GP zones per one mole of Mg atoms is 4 mol, 2 mol and 4/3 mol for Al_3Mg, AlMg and $AlMg_3$, respectively. The overall change in enthalpy by forming a GP zone out of 1 mol magnesium is −1.32 kJ, −1.30 kJ and −0.85 kJ. This means that the Al_3Mg zones are therefore preferred in Al-rich alloys due to the limiting Mg content. Previously, GP zones with 25% of Mg have been observed experimentally in supersaturated Al solid solutions [32, 35].

There is a temperature-composition dependence for the formation of Al_3Mg GP zones. To map this relationship, we computed the point at which GP zones start to form by tracking the phase boundary between Al and Al_3Mg in the FCC lattice. Figure 2b shows for low Mg concentrations that the system is characterised by dispersed magnesium atoms within the Al matrix. As the Mg concentration becomes sufficiently high, Al_3Mg zones start to form. For example, at 293 K, we find that clusters start to form at about 3% of Mg. Our results suggest that the clusters start to form at slightly lower compositions than what was found experimentally, but the result is rather close and highlights the applicability of this computational approach in nucleation studies.

After knowing the phase separation line and the region of co-existence, one can also compute the free energy barriers for forming GP zones. Figure 6 shows that the system can lower its energy by forming Al_3Mg zones of any size, meaning that two Mg atoms will always prefer Al_3Mg over being dissolved in the Al matrix. Even after including the contribution from strain fields caused by the lattice mismatch between the two phases, the cluster remains stable for all sizes. However, including the contribution of entropy (figure 8a) results in that the free energy actually increases for small cluster sizes. This highlights the two effects that one intuitively expects to be present. First, if the solute concentration is low, GP zones are less likely to form. Secondly, if the temperature becomes too high the solubility of Mg in Al increases and Mg atoms tend to be dispersed in the Al matrix. As shown in Equation (9), the change in entropy makes the free energy barrier large both when the solute concentration is small, and when the temperature becomes high.

The aforementioned fact that interfacial energy is not large enough to produce a barrier, can be understood by considering the local environment of each Mg atom in both phases. Once an Mg atom is in the diluted phase, all its neighbours are (naturally) Al atoms. But the same is true also in the Al_3Mg phase due to the $L1_2$ structure, and hence, the first difference between these to phases can be observed in the second nearest neighbour interaction. As a consequence of the similarities in the local environment each Mg atom experience, it is not surprising that the interfacial energy turns out to have a rather weak contribution in the overall free energy.

In the present work, the nucleation model developed by Kamijo *et al.* [24] was applied. The main benefit of using Kamijo's model, is that the free energy of the cluster can be obtained from the ground state energy. Moreover, since the temperature and solute concentration dependency enters in the analytical approximation of the entropy one can trivially obtain the free energy change associated with cluster formation at all temperatures and solute compositions. However, as the change in entropy results in a free energy barrier, one may ask whether a cluster with higher configurational entropy (e.g. a disordered

cluster) has a lower barrier? There are two types of disorder that can occur for a cluster embedded in a matrix: ordering defects within the bulk of the cluster and disorder on the cluster-matrix interface. We separate these two contributions by first considering free energy of a pure Al_3Mg phase. At 293 K, we find a lowering of the free energy by 1.6 meV/f.u. and an entropy of $\Delta S_B = 0.036$ meV/f.u./K. Assuming that the critical cluster size is much larger than 1, the entropy change in Kamijo's model is $\Delta S_K \approx k_B N \ln c_{Mg}$, where N is the number of formula units. Hence, the ratio between the entropy change from the analytical model and the correction due to weak distortions inside the bulk is $(\Delta S_K/\Delta S_B)$ is 7 and 11 at 5% and 1% solute composition, respectively. Thus, the correction attributed to distortion within the bulk of the cluster adds up only a small correction to the analytical model.

To quantify the surface entropy of the cluster we performed a MC calculations where all Mg atoms are forced to be connected by second nearest neighbour pairs. In this kind of calculations, the lowering of free energy with increasing temperature is caused by deviations from the perfect cubic ground state cluster. We found that clusters start to deviate from the cubic structures already around 100 K. As depicted in figure 8a, the entropic contribution significantly influences the barrier obtained from Kamijo's model. However, we emphasise that at low solute concentration the entropy loss in the analytical model is indeed the dominating term. Therefore, it is possible to obtain good approximations of the free energy barriers based solely on 0 K data, provided that the solute concentration is low.

In the framework of the transition state theory (TST), the rate at which products form is directly proportional to $\exp(-\beta\Delta F^*)$, where ΔF^* is the free energy barrier separating reactants and products [41]. In this case, GP zones are the products and cases with solute atoms dispersed in the Al-matrix are the reactants. $\exp(-\beta\Delta F^*)$ can be interpreted as the probability of observing the system in a transition state on the top of the free energy barrier relative to observing the system in a state where the Mg atoms are fully dispersed. Thus, the probability of occupying a transition state approaches zero as the concentration gets low or when the temperature becomes high. Consequently, GP zones are unlikely to form in either of these conditions as demonstrated in figure 8. If the solute concentration fluctuates within the sample, the strong composition dependence of the barrier suggests that GP zones are more likely to form in solute rich regions. Hence, our results suggest that in the early stage of the precipitate formation process, stable GP zones first appear in regions with enriched solute concentration. Thus, it is essential to consider spatial variations in the solute concentration when modelling clustering in alloys. Further knowledge of the barrier is valuable not only for equilibrium studies, but also as input for rate constants in kinetic modelling of precipitate formation.

6. Conclusion

We have studied the Al-Mg phase diagram and initial clustering of GP zones using the Cluster Expansion formalism for atomistic MC simulations. The achieved accuracy for our CE-MC simulations is of the order of 1 meV/atom in comparison with DFT. The simulations performed for three phases Al-Mg (FCC, HCP, γ-phase) confirm the experimental knowledge of the relative stabilities of these phases at different concentrations while also providing information on their temperature-dependence, and the mapping of phase boundaries (for nucleation) on the Al-rich side provides results in a good agreement with experiments. Our simulations demonstrate that ordered zones with 25% of Mg ($L1_2$ phase) will form in Al-rich alloys provided that the overall Mg concentration is high enough. We have also computed the metastable phase diagram which shows the temperatures where GP zones dissolve at all relevant compositions. The simulations suggest that GP zones are stable at slightly higher temperatures ($\sim$ 50 K) than what has been detected in experiments. At last, we calculated the free energy barriers associated with the formation of GP zones as a function of size, solute composition and temperature, and noted that the inclusion of entropy (in free energy) leads to a qualitative change in energetics. Without entropy, the Al_3Mg clusters are stable at all sizes, while entropy yields free energy profiles with barriers at critical cluster sizes. Crossing such a barrier is a prerequisite for a GP zone growth, as in the classical nucleation theory.

In this work, all DFT energies were extracted from fully relaxed atomistic structures and unit cells at each composition. As limitations of our model, we note that it does not include vibrational entropy and thermal expansion (0 K data in the DFT training set), and it does not consider vacancies which are crucial in further precipitate formation (from GP zones). We estimated the energy contributions from strain fields based on Eshelby's inclusion theory and added them in a post processing step. Vacancies and incorporation of strain energy in Monte Carlo calculations will be topics for future work to further develop the CE-MC formalism to extract thermodynamic information of the precipitate formation process from atomistic simulations.

7. Acknowledgments

The DFT simulations were performed on resources provided by UNINETT Sigma2 - the National Infrastructure for High Performance Computing and Data Storage in Norway. We also thank Jin Hyun Chang and Juan Maria Garcia Lastra for their effort in developing the cluster expansion module.

8. References

[1] D. Carle and G. Blount. The suitability of aluminium as an alternative material for car bodies. *Materials & design*, 20(5):267–272, 1999.

[2] E. A. Starke and J. T. Staley. Application of modern aluminum alloys to aircraft. *Progress in Aerospace Sciences*, 32(2-3):131–172, 1996.

[3] C. D. Marioara, S. J. Andersen, J. Jansen, and H. W. Zandbergen. Atomic model for GP-zones in a 6082 Al–Mg–Si system. *Acta Materialia*, 49(2): 321–328, 2001.

[4] S. J. Andersen, H. W. Zandbergen, J. Jansen, C. Traeholt, U. Tundal, and O. Reiso. The crystal structure of the β-phase in Al–Mg–Si alloys. *Acta Materialia*, 46(9):3283–3298, 1998.

[5] C. D. Marioara, S. J. Andersen, H. W. Zandbergen, and R. Holmestad. The influence of alloy composition on precipitates of the Al–Mg–Si system. *Metallurgical and Materials Transactions A*, 36(3):691–702, 2005.

[6] S. Wenner, J. Friis, C. D. Marioara, and R. Holmestad. Precipitation in a mixed Al–Cu–Mg/Al–Zn–Mg alloy system. *Journal of Alloys and Compounds*, 684:195–200, 2016.

[7] J. P. Lynch, L. M. Brown, and M. H. Jacobs. Microanalysis of age-hardening precipitates in aluminium alloys. *Acta Metallurgica*, 30(7): 1389–1395, 1982.

[8] T. J. Bastow and S. Celotto. Clustering and formation of nano-precipitates in dilute aluminium and magnesium alloys. *Materials Science and Engineering: C*, 23(6-8):757–762, 2003.

[9] J. M. Sanchez. Cluster expansions and the configurational energy of alloys. *Physical review B*, 48(18):14013, 1993.

[10] J. Teeriniemi, J. Huisman, P. Taskinen, and K. Laasonen. First-principles modelling of solid Ni–Rh (nickel–rhodium) alloys. *Journal of Alloys and Compounds*, 652:371–378, 2015.

[11] J. Teeriniemi, M. Melander, S. Lipasti, R. Hatz, and K. Laasonen. Fe–Ni nanoparticles: A multiscale first-principles study to predict geometry, structure, and catalytic activity. *The Journal of Physical Chemistry C*, 121 (3):1667–1674, 2017.

[12] J. Teeriniemi, P. Taskinen, and K. Laasonen. First-principles investigation of the Cu–Ni, Cu–Pd, and Ni–Pd binary alloy systems. *Intermetallics*, 57: 41–50, 2015.

[13] M. Asta, V. Ozolins, and C. Woodward. A first-principles approach to modeling alloy phase equilibria. *JOM*, 53(9):16–19, 2001.

[14] A. R. Natarajan, E. Solomon, B. Puchala, E. A. Marquis, and A. Van der Ven. On the early stages of precipitation in dilute Mg–Nd alloys. *Acta Materialia*, 108:367–379, 2016.

[15] A. V. Ruban and I. A. Abrikosov. Configurational thermodynamics of alloys from first principles: effective cluster interactions. *Reports on Progress in Physics*, 71(4):046501, 2008.

[16] S. Samson. The crystal structure of the phase β-Mg_2Al_3. *Acta Crystallographica*, 19(3):401–413, 1965.

[17] W. Steurer. The Samson phase, β-Mg_2Al_3, revisited. *Zeitschrift für Kristallographie*, 222(6):259–288, 2007.

[18] M. Murayama, K. Hono, M. Saga, and M. Kikuchi. Atom probe studies on the early stages of precipitation in Al–Mg–Si alloys. *Materials Science and Engineering: A*, 250(1):127–132, 1998.

[19] L. J. Nelson, V. Ozoliņš, C. S. Reese, F. Zhou, and G. Hart. Cluster expansion made easy with bayesian compressive sensing. *Physical Review B*, 88(15):155105, 2013.

[20] A. Seko, Y. Koyama, and I. Tanaka. Cluster expansion method for multi-component systems based on optimal selection of structures for density-functional theory calculations. *Physical Review B*, 80(16):165122, 2009.

[21] M. E. J. Newman and G. T. Barkema. *Monte Carlo Methods in Statistical Physics chapter 1-4*. Oxford University Press: New York, USA, 1999.

[22] A. Van de Walle and M. Asta. Self-driven lattice-model monte carlo simulations of alloy thermodynamic properties and phase diagrams. *Modelling and Simulation in Materials Science and Engineering*, 10(5):521, 2002.

[23] R. P. Sear. Nucleation: theory and applications to protein solutions and colloidal suspensions. *Journal of Physics: Condensed Matter*, 19(3): 033101, 2007.

[24] T. Kamijo and H. Fukutomi. A new theory of the homogeneous nucleation of a coherent precipitate. *Philosophical Magazine A*, 48(5):685–693, 1983.

[25] A. Seko, S. R. Nishitani, I. Tanaka, H. Adachi, and E. F. Fujita. First-principles calculation on free energy of precipitate nucleation. *Calphad*, 28(2):173–176, 2004.

[26] J. D. Eshelby. The determination of the elastic field of an ellipsoidal inclusion, and related problems. *Proc. R. Soc. Lond. A*, 241(1226):376–396, 1957.

[27] M. De Jong, W. Chen, T. Angsten, A. Jain, R. Notestine, A. Gamst, M. Sluiter, C. K. Ande, S Van Der Zwaag, JJ Plata, et al. Charting the complete elastic properties of inorganic crystalline compounds. *Scientific data*, 2:150009, 2015.

[28] J. J. Mortensen, L. B. Hansen, and K. W. Jacobsen. Real-space grid implementation of the projector augmented wave method. *Physical Review B*, 71(3):035109, 2005.

[29] J. Enkovaara, C. Rostgaard, J. J. Mortensen, J. Chen, M. Dułak, L. Ferrighi, J. Gavnholt, C. Glinsvad, V. Haikola, H. A. Hansen, et al. Electronic structure calculations with GPAW: a real-space implementation of the projector augmented-wave method. *Journal of Physics: Condensed Matter*, 22(25):253202, 2010.

[30] A. H. Larsen, J. J. Mortensen, J. Blomqvist, I. E. Castelli, R. Christensen, M. Dułak, J. Friis, M. N. Groves, B. Hammer, C. Hargus, et al. The atomic simulation environment – a python library for working with atoms. *Journal of Physics: Condensed Matter*, 29(27):273002, 2017.

[31] J. P. Perdew, K. Burke, and M. Ernzerhof. Generalized gradient approximation made simple. *Physical review letters*, 77(18):3865, 1996.

[32] J. L. Murray. The Al–Mg (aluminum- magnesium) system. *Journal of Phase Equilibria*, 3(1):60–74, 1982.

[33] J. H. Chang, D. Kleiven, M. Melander, J. Akola, J. Lastra, and T. Vegge. CLEASE: A versatile and user-friendly implementation of cluster expansion method. *arXiv preprint arXiv:1810.12816*, 2018.

[34] M. E. J. Newman and R. M. Ziff. Fast monte carlo algorithm for site or bond percolation. *Physical Review E*, 64(1):016706, 2001.

[35] C. Gault, A. Dauger, and P. Boch. Decomposition of aluminium-magnesium solid solutions studied by ultrasonic measurements of elastic properties and electron microscopy. *Acta Metallurgica*, 28(1):51–60, 1980.

[36] K. Osamura and T. Ogura. Metastable phases in the early stage of precipitation in Al–Mg alloys. *Metallurgical Transactions A*, 15(5):835–842, 1984.

[37] T. Sato, Y. Kojima, and T. Takahashi. Modulated structures and GP zones in Al–Mg alloys. *Metallurgical Transactions A*, 13(8):1373–1378, 1982.

[38] V. Fallah, N. Ofori-Opoku, J. Stolle, N. Provatas, and S. Esmaeili. Simulation of early-stage clustering in ternary metal alloys using the phase-field crystal method. *Acta Materialia*, 61(10):3653–3666, 2013.

[39] F. Bakare, M. I. Babalola, and B. E. Iyorzor. The role of alloying elements on the structural, mechanical and thermodynamic properties of Al3X binary alloy system (X= Mg, Sc and Zr): first principle calculations. *Materials Research Express*, 4(11):116502, 2017.

[40] C. Wolverton. First-principles theory of 250 000-atom coherent alloy microstructure. *Modelling and Simulation in Materials Science and Engineering*, 8(3):323, 2000.

[41] H. Eyring. The activated complex and the absolute rate of chemical reactions. *Chemical Reviews*, 17(1):65–77, 1935.